Università degli studi di Udine

Dependability Assessment of Transfer Length Method to Extract the Metal–Graphene Contact Resistance

Original

Availability:
This version is available http://hdl.handle.net/11390/1181642 since 2020-05-08T14:03:17Z

Publisher:

Published
DOI:10.1109/TSM.2020.2981199

Terms of use:
The institutional repository of the University of Udine (http://air.uniud.it) is provided by ARIC services. The aim is to enable open access to all the world.

Publisher copyright

(Article begins on next page)

25 April 2024

Dependability assessment of Transfer Length Method to extract the metal–graphene contact resistance

Francesco Driussi*, Stefano Venica*, Amit Gahoi†, Satender Kataria†, Max C. Lemme†‡, Pierpaolo Palestri*

***Abstract*—The measurement of the contact resistance (R_C) in semiconductor devices relies on the well–established Transfer Length Method (TLM). However, an in–depth investigation on its applicability to characterize the metal–graphene contacts is still missing. In this work, a dependability analysis on the R_C values extracted from several metal–graphene stacks is performed, also devising strategies to limit the large observed statistical errors and to obtain dependable results. In particular, artifacts due to an incorrect application of TLM, e.g. negative resistance values, can be eliminated. Finally, a simulation study is proposed to quantify the contribution to R_C of the so–called junction resistance at the edge of the contact, that some authors in the literature invoke to explain the observed artifacts.**

***Index Terms*—Graphene, contact resistance, Transfer Lenght Method, measurement reliability, junction resistance, modeling.**

I. INTRODUCTION

TWO–dimentional (2D) materials are largely investigated as possible boosters/enablers for "more than Moore" technologies [1]. As an example, the high mobility and electron velocity in graphene make graphene–FETs (GFETs) promising for high performance RF analog circuits [2]. Indeed, nowadays GFET cut–off frequencies are comparable with those of state–of–the–art RF transistors [3]. Furthermore, graphene is excellent for many other applications such as fast photodetectors [4], NEMS/MEMS and sensors [5], terahertz modulators [6], supercapacitors [7] and displays [8].

However, the performance of all these devices is largely hampered by the large Metal–Graphene (M–G) contact resistance (R_C) [9]. For instance, it strongly limits the maximum oscillation frequency of GFETs and also of alternative device concepts based on 2D materials [2], [10]–[12].

Despite the efforts spent to improve the quality of the M–G contacts [13], a further breakthrough in the engineering of the M–G junction to lower R_C is mandatory to boost graphene technology. However, this cannot be achieved without an in–depth understanding of the physics behind the conduction mechanism across the M–G stack and this is possible only through reliable experimental techniques allowing the assessment of the M–G stack nature [14], [15].

* Universitá degli Studi di Udine, Dipartimento Politecnico di Ingegneria e Architettura (DPIA), via delle Scienze 206, 33100 Udine, Italy (email: venica.stefano@spes.uniud.it).

† Chair of Electronic Devices, Faculty of Electrical Engineering and Information Technology, RWTH Aachen University, Otto-Blumenthal-Str. 25, 52074 Aachen, Germany.

‡ AMO GmbH, Advanced Microelectronic Center Aachen, Otto–Blumenthal–Str. 25, 52074 Aachen, Germany.

The work was partially funded by the EU through the FP7–ICT STREP Project "GRADE" (grant 317839) via the IU.NET consortium, by the Italian MIUR through the PRIN project "Five2D" (2017SRYEJH), by the German Ministry of Education and Research (BMBF) through the grant "GIMMIK" (03XP0210) and by the Graphene Flagship (785219).

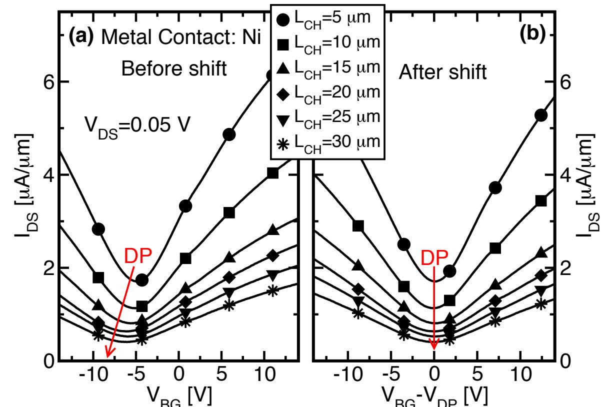

Fig. 1. (a) Typical current vs. V_{BG} curves of GFETs of a TLM structure with $W = 20$ μm and Ni contacts. All GFETs show a DP at V_{DP}<0, with a value slightly depending on L_{CH}. (b) Transfer characteristics are shifted to align the DP positions.

In semiconductor technology, the Transfer Length Method (TLM) has been routinely used to measure R_C between metals and semiconductor materials [14]. However, the applicability of TLM to graphene devices and the correctness of the obtained R_C values have not been deeply investigated yet. Indeed, the R_C data for M–G contacts reported in the literature are characterized by large error bars [15] and, in several cases, by negative R_C values [16]–[20]. Often the authors impute these negative R_C values to the metal–induced doping of the graphene underneath or in proximity of the contacts, that translates in the so–called junction resistance (R_{JUN}) at the edge between the metal contact and the GFET channel. R_{JUN} is due to different graphene charge densities in the channel and underneath the contact region [21].

In this paper, an in–depth assessment of R_C extracted through TLM is presented and strategies to limit the observed errors are proposed, thus leading to dependable M–G contact resistance values. Furthermore, the work of [22] is extended by using semi–classical Monte–Carlo (MC) simulations to evaluate the effect of the metal–induced doping of graphene and the contribution of R_{JUN} to R_C, with the aim to solve the open question concerning the origin of the negative R_C values reported in the literature.

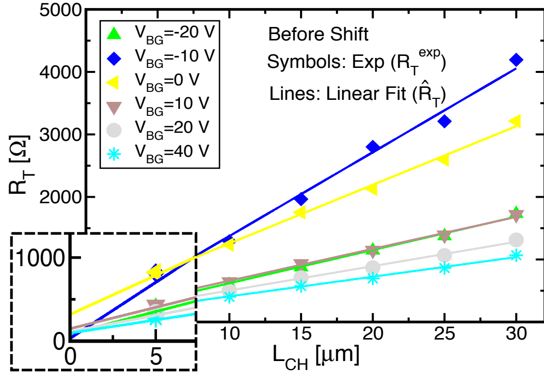

Fig. 2. Total resistance R_T^{exp} (symbols) versus L_{CH} obtained from the data in Fig. 1(a) at different V_{BG}. Linear regression (lines) allows to extract R_{SH} and R_C. The zoom near the origin of the axis highlights the intercept value ($2R_C$).

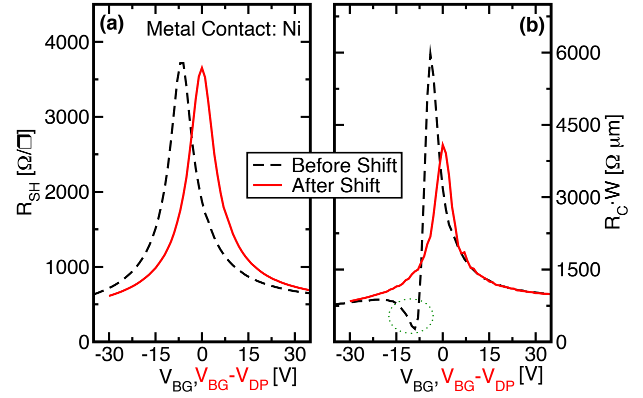

Fig. 3. Sheet resistance (a) and contact resistance (b) versus V_{BG} (dashed lines) extracted from the linear fittings in Fig. 2. Near the DP, R_C shows an evident drop (highlighted area). The shifted transfer charateristics in Fig. 1(b) lead to a very different R_C behavior and the dip disappears.

II. Fabricated TLM structures and experimental procedure

The measured TLM test structures consist of a series of back–gated GFETs with different width (W) and a channel length (L_{CH}) that ranges from 5 to 50 μm. Boron–doped (p–type) silicon substrates have been thermally oxidized to obtain an 85 nm SiO_2 back oxide, on top of which a monolayer CVD graphene is tranferred. To make the contacts, nickel (Ni), copper (Cu) or gold (Au) were used. The complete fabrication process flow of the TLM structures can be found in [23].

The samples were characterized in DC at 300 K in a Lake Shore Cryotronics probestation to ensure ultra–high vacuum conditions ($< 10^6$ mbar). The source–drain currents (I_{DS}) of the GFETs with different L_{CH} are routinely measured as a function of the applied back–gate bias (V_{BG}). Fig. 1(a) reports the typical results for a TLM sample with Ni contacts. The Dirac Point (DP), i.e. the minimum conduction point, is clearly visible and, for this sample, it is located at negative back–gate voltages ($V_{DP} < 0$ V). Furthermore, V_{DP} slightly depends on L_{CH} and this can be due to some unintentional graphene doping/interfacial impurities and/or to residual air/humidity that shift the DP position with respect to zero [24].

III. Experimental M–G contact resistance

The measured transfer characteristics have been used to calculate the total resistance R_T^{exp} of each GFET. It is generally assumed that R_T^{exp} is contributed by the channel resistance, the M–G contact resistance R_C and the resistance of the metallic electrode (this latter is typically neglected) [14]. If the sheet resistance R_{SH} of the graphene layer is uniform in the whole TLM structure, R_T^{exp} linearly depends on L_{CH}, as:

$$R_T^{exp} = \frac{V_{DS}}{I_{DS}} = \frac{R_{SH}}{W} L_{CH} + 2R_C. \quad (1)$$

R_T^{exp} is calculated for the data in Fig. 1(a), obtaining the R_T^{exp} versus L_{CH} curves of Fig. 2 (symbols). According to Eq. 1, R_{SH} and R_C are extracted from the slope and the intercept with the y–axes of the linear regression (lines), respectively. The zoomed area near the origin of the axis highlights the $2R_C$ value, that appears to be non–monotonic with $|V_{BG}|$ and rapidly drops for $V_{BG} = -10$ V (blue line).

The R_{SH} and R_C versus V_{BG} values extracted from Fig. 2 are reported in Fig. 3 (dashed lines). R_{SH} (a) shows the typical bell–shape behavior of graphene channels (large resistivity near the DP). Instead, the extracted R_C (b) shows a clear dip at $V_{BG} \simeq -10$ V similar to those previously reported in the literature [15]–[17].

A. Statistical errors in the extracted R_C

In order to assess the correctness of the data in Fig. 3 (dashed lines), the statistical errors related to the R_{SH} and R_C extraction are calculated. In particular, the regression coefficient (r^2) and the errors (ε) caused by the linear regression in Fig. 2 are [25]:

$$r^2 = 1 - \frac{\sum_i^N (R_T^{exp} - \widehat{R}_{T_i})^2}{\sum_i^N (R_T^{exp} - \overline{R}_T)^2} \quad (2)$$

$$\varepsilon(R_{SH}) = \pm\, W \sqrt{\frac{\sigma^2}{S_{xx}}} \quad (3)$$

$$\varepsilon(R_C) = \pm\, \frac{1}{2} \sqrt{\sigma^2 \left[\frac{1}{N} + \frac{\overline{L_{CH}}}{S_{xx}}\right]}, \quad (4)$$

where:

$$\sigma^2 = \frac{\sum_i^N (R_{T_i}^{exp} - \widehat{R}_{T_i})}{N-2} \quad (5)$$

$$S_{xx} = \sum_i^N (L_{CH_i} - \overline{L_{CH}})^2 \quad (6)$$

$$\widehat{R}_{T_i} = \frac{R_{SH}}{W} L_{CH_i} + 2R_C. \quad (7)$$

The calculated r^2 is very close to one ($r^2 > 0.987$), although it reduces near the DP (see [22]). Also the R_{SH} error reported in Fig. 4(a, dashed line) is quite small, supporting the correctness of the extracted R_{SH} data.

Instead, the relative error for R_C reported in Fig. 4(b, dashed line) is very huge, especially in correspondence of

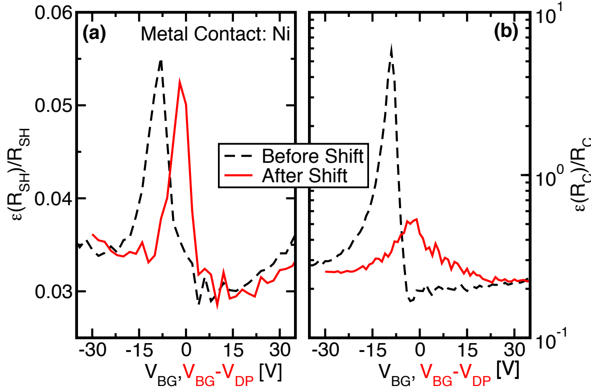

Fig. 4. Relative error on R_{SH} (a) and on R_C (b) versus V_{BG} calculated applying Eqs. 3–7 to the data in Fig. 2. The error is small for R_{SH}, while it is huge for R_C at $V_{BG} \approx -10$ V. The transfer characteristics versus $(V_{BG}-V_{DP})$ in Fig. 1(b) lead to much smaller errors (solid lines), especially near the DP.

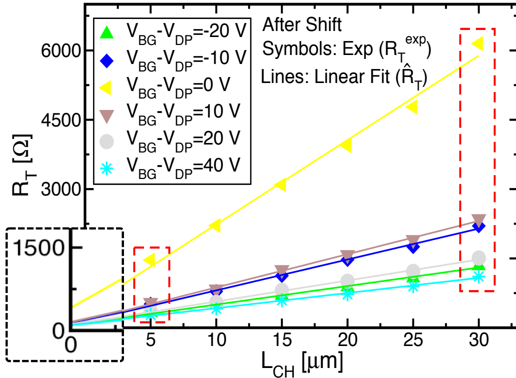

Fig. 5. Experimental R_T^{exp} (symbols) as a function of L_{CH} at different $(V_{BG} - V_{DP})$ obtained from the curves reported in Fig. 1(b). The shortest and longest devices (5 and 30 μm) are potentially responsible for the errors in the DP proximity seen in Fig. 4(b).

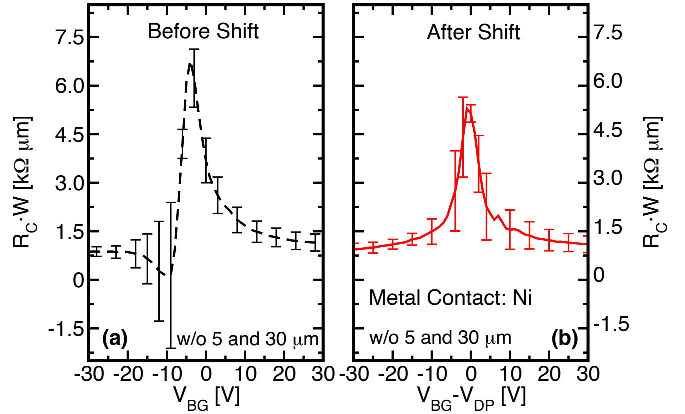

Fig. 6. R_C characteristics with the corresponding error bars $[\pm\varepsilon(R_C)]$ obtained excluding the outliers. Data are extracted considering the original (a) and the shifted transfer characteristics (b). The latter can be considered as the most dependable result.

the dip in the R_C curve of Fig. 3(b) (close to the DP). This extremely large error can be due to the small L_{CH} dependence of the DP position in the curves of Fig. 1(a). To verify this, the currents of each GFET as a function of $(V_{BG} - V_{DP})$ are re–plotted in Fig. 1(b), thus compensating the slightly different V_{DP} in the measured devices. In this way, R_T^{exp} of the different GFETs is compared at the same charge carrier concentration in the graphene channels. The R_{SH} and R_C are now extracted from the shifted I_{DS} curves of Fig. 1(b).

Figure 5 shows R_T^{exp} versus L_{CH} curves obtained at given $(V_{BG} - V_{DP})$ values. Differently from Fig. 2, by looking at the zoomed area, the intercept of the linear regression is now monotonic with $|V_{BG} - V_{DP}|$. Furthermore, Fig. 3 compares the newly extracted R_{SH} and R_C values (red solid lines) with those (black dashed lines) extracted from the initial I_{DS}–V_{BG} curves. R_{SH} is pretty similar, as it is similar the R_{SH} statistical error made by using both the original and shifted IV curves [Fig. 4(a)].

Instead, R_C is very different from the previous extraction and the dip near the DP disappears. Furthermore, these new R_C values are characterized by a much smaller relative error [Fig. 4(b), solid line], making the extracted R_C values much more robust.

By carefully observing the R_T^{exp} vs. L_{CH} curves in Fig. 5, it is also possible to note that some points slightly deviate from the linear behavior ($L_{CH} = 5$; 30 μm, red dashed box). In [22], it has been verified that the exclusion of these outliers from the linear regression indeed improves r^2 and the R_C error related to the extraction procedure. However, it has been also demonstrated that the huge error in Fig. 4(b) (dashed line, especially at $V_{BG} \approx V_{DP}$) is mainly due to the DP variation between the GFETs in the TLM structure (see Fig. 6). Hence, the compensation of the V_{DP} variability among the I_{DS} characteristics is mandatory to obtain dependable R_C and it is much more important than the identification of possible outliers. Anyway, to further improve the dependability of the R_C results, the extraction procedure is run also by excluding the GFETs with $L_{CH} = 5$ μm and 30 μm of the investigated TLM structure with Ni–graphene contacts and Fig. 6(b) shows the obtained R_C with the corresponding error bars. Even by considering these error bars, the calculated R_C is always positive.

B. Contact resistance for different metal materials

The validity of the developed extraction procedure has been verified also on TLM structures with different metal contacts. Indeed, the issue related to the V_{DP} position varying along the TLM structure is observed also in the samples with Au and Cu contacts, as also reported in [22]. As a reference, the R_C values are first extracted by using the raw I_{DS}–V_{BG} curves measured in the samples [Fig. 7(a)]. All the curves peak at the DP position ($V_{DP} < 0$ for Ni and Au; $V_{DP} > 0$ for Cu, see Fig. 12 of [22]), but they show different and somewhat distorted shapes with dips and also negative R_C values for the Au sample.

In this respect, the relative R_C error is unacceptably large for all the metals, with values up to 600% for Ni and Au [see Fig. 7(b)]. In general, the error is very large in correspondence of distortions and dips in the R_C curves and, in particular, when R_C becomes negative in the Au sample.

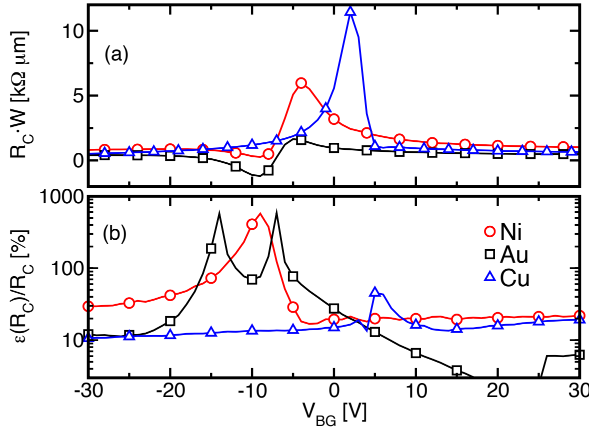

Fig. 7. (a) R_C obtained from TLM structures with different metal contacts by using the raw I_{DS}–V_{BG} characteristics. The curves show artifacts and distortions, such as negative R_C values for the Au contact. (b) For all the metal materials, the statistical error related to the R_C extraction is huge and unacceptable.

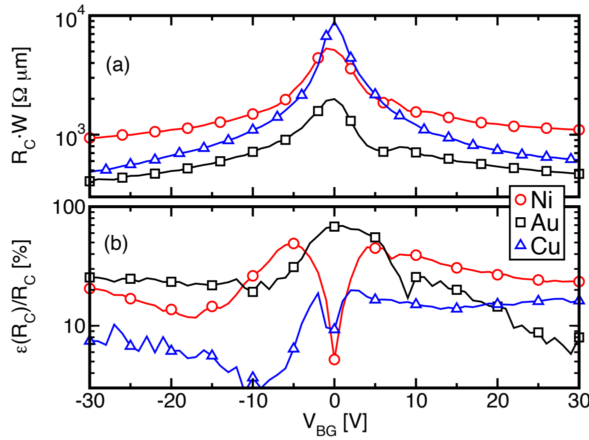

Fig. 8. (a) R_C obtained from TLM structures with different metal contacts by using the developed procedure, namely by compensating the V_{DP} variability and excluding the outliers. The R_C curves show the typical bell–shape. (b) For all the metals, now the R_C statistical error is much smaller than before.

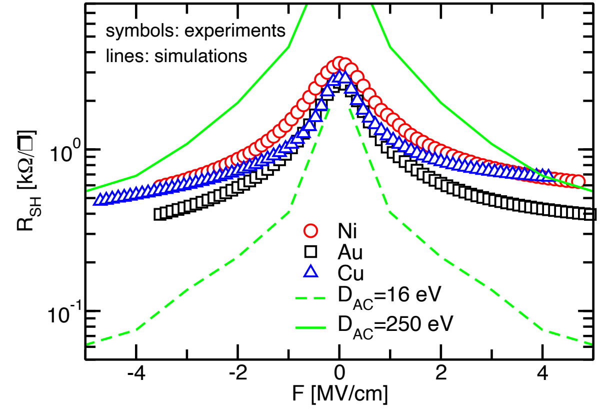

Fig. 9. R_{SH} vs. the back–oxide electric field F extracted from TLM structures by using the developed procedure (symbols). The curves show the typical bell–shape of graphene channels. The samples with different metal contacts show similar graphene quality. For comparison, MC simulations assuming two values of the deformation potential of acoustic phonons (D_{AC}) are also reported (lines).

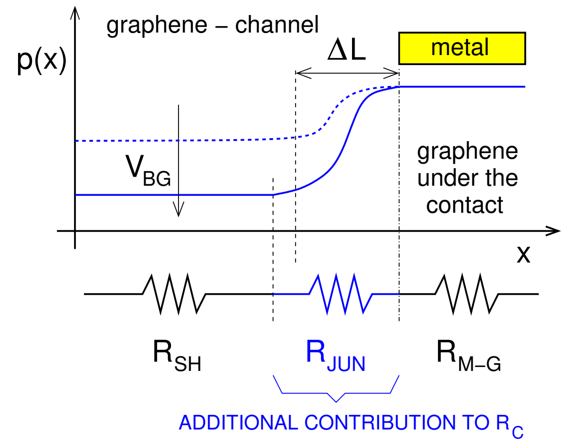

Fig. 10. Sketch of the hole density profile in the graphene layer along the transport direction in proximity of the Au contact. The step between the channel and the region under the metal (higher at large V_{BG}) leads to a p–p+ junction. The associated junction resistance R_{JUN} adds to the resistance R_{M-G} due to the sole M–G stack.

To reduce the R_C extraction error, the V_{DP} variation is compensated among the IV curves of GFETs in the same TLM structure and the outliers from the linear regression of R_T versus L_{CH} data are excluded. The R_C results in Fig. 8(a) are obtained following this procedure and they are characterized by much lower errors than before [although not very small close to the DP, see Fig. 8(b)]. So now the extracted R_C can be considered dependable and all curves show the bell–shape behavior typical of graphene channels. It is worth noticing that Ni contacts exhibit the highest R_C (except at the DP position), while Au contacts show the lowest R_C values [9].

Figure 9 (symbols) finally reports the extracted R_{SH} values as a function of the back–oxide electric field F for the TLM samples with the different metals, demonstrating the similar quality of the graphene in the measured samples.

IV. MC SIMULATIONS OF THE JUNCTION RESISTANCE

As mentioned in Sec. I, the negative R_C reported in the literature is often ascribed to the metal–induced doping of the graphene underneath or in proximity of the contact [16]–[20]. Indeed, metals electrostatically dope graphene [9], inducing different charge concentrations between the graphene channel and the region underneath the contact and possibly forming a pseudojunction [21]. As an example, graphene is p–doped by Au contacts [9] and p–p+ or n–p+ junctions may appear near the contact edge, depending on the applied V_{BG} value (it drives the graphene channel charge, see Fig. 10).

This pseudojunction has a twofold effect: 1) it leads to a *junction* resistance (R_{JUN}) that depends on V_{BG} and contributes to the series resistance in the GFETs; 2) it extends into the channel (ΔL, Fig. 10) and shortens the portion of graphene with uniform charge density and characterized by R_{SH}. Hence, Eq. 1 must be re–written as:

$$R_T^{exp} = \frac{R_{SH}}{W}(L_{CH} - 2\Delta L) + 2(R_{JUN} + R_{M-G}), \quad (8)$$

where R_{M-G} is the actual contact resistance of the sole M–G

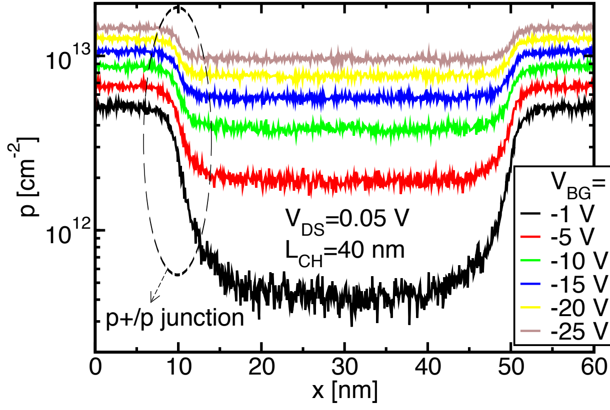

Fig. 11. Hole density along the GFET for different V_{BG} values calculated with the MC simulator. Near the contact edge, the p–$p+$ junction is higlighted.

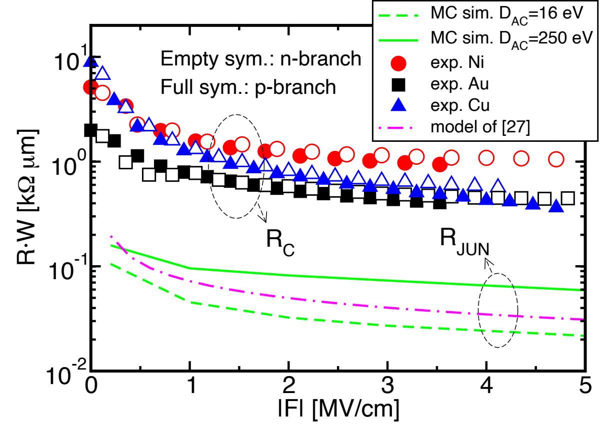

Fig. 12. Experimental R_C (symbols) compared with R_{JUN} simulated with the MC model (green lines) for two D_{AC} values. As a reference, the R_{JUN} is calculated also with the ballistic model of [27], namely $R_{JUN} = \frac{\pi^2 \hbar^2 v_F}{2q^2(E_F - E_{DP})}$, where v_F, E_F and E_{DP} are, respectively, the Fermi velocity, the Fermi level and the DP energy level in the graphene channel, since this latter is the bottleneck for the carrier transport in the pseudojunction at the contact edge.

stack (Fig. 10). R_T^{exp} is still proportional to L_{CH} and R_C is extrapolated at $L_{CH} = 0$, leading to:

$$R_C = -\frac{R_{SH}}{W}\Delta L + R_{JUN} + R_{M-G}. \quad (9)$$

Close to V_{DP}, the charge density in the channel is rather low and, by assuming that the metal is anyway inducing a large graphene doping under the contact, this high charge step may lead to large R_{JUN} and ΔL and, thus, to a R_C value very different from the actual R_{M-G}. This assumption has been used in the literature to justify the reported negative R_C values near the DP. Indeed, the first term in Eq. 9 can produce, in some cases, negative R_C, depending on the R_{JUN}, ΔL and R_{M-G} values. To investigate on this point and to evaluate the R_{JUN} contribution to R_T of GFETs, Monte-Carlo (MC) simulations of the charge density profile along the GFET have been performed.

The MC simulator couples self–consistently the Boltzamnn transport equation for electrons and holes in the graphene channel to the non–linear Poisson equation [26]. For graphene, it considers a gapless energy dispersion relationship, scattering with acoustic and optical phonons and band-to-band tunneling. Remote phonon scattering in the top–oxide and back–oxide is also considered. Concerning source/drain regions, the simulator can model either chemical or electrostatic doping. The latter relates to the M–G interactions [9] and the tool calculates the metal–induced displacement with respect to DP of the Fermi level in the graphene underneath the contact. Furthermore, the model also accounts for the voltage drop across R_{M-G} and its impact on the GFET current. More details on the MC model can be found in [26].

Figure 11 shows the hole density along the GFET length calculated with the MC simulator. In this plot, Au contacts with a workfunction of 5.2 eV has been assumed, so that they p–dope the underneath graphene [9]. Lowering V_{BG}, more holes are accumulated in the graphene channel and the step in hole concentration at the contact edge is reduced. Note that the extension of the p–$p+$ junction is rather limited, resulting in $\Delta L < 10$ nm for all the simulated V_{BG} values [27]–[30]. This is in agreement with the fact that the metal–induced doping vanishes within a few nanometers [9], [31].

It is worth mentioning that we consider these simulations as a worst case, since Ni and Cu have workfunctions (5 eV and 4.7 eV, respectively) that are lower than Au and closer to the graphene electron affinity (4.6 eV), so smaller charge density steps are expected for the Ni and Cu cases.

To calculate the R_{JUN} values, GFETs with different L_{CH} are simulated by imposing $R_{M-G} = 0$ in the MC model (see Eq. 9). Then the simulated R_{SH} and R_{JUN} are extracted again via the linear fitting of the GFET resistance vs. L_{CH} curves. Figure 9 (lines) directly reports the MC results for R_{SH}. By assuming standard graphene scattering parameters (dashed line), the simulated R_{SH} is smaller than in the experiments, especially at large magnitudes of the vertical electric field $|F|$. This may reflect a non ideal graphene quality, with increased scattering. To the sole purpose of reproducing the experiments with the model, the deformation potential D_{AC} of the acoustic phonons is empirically increased (solid line). Now simulations are much closer to the measurements for large $|F|$ values, although the simulated R_{SH} is larger close to the DP (at $F = 0$). By assuming the two D_{AC} values in Fig. 9, the R_{JUN} curves in Fig. 12 (green lines) are obtained, that are rather consistent with the data of the ballistic model for pseudojunctions in graphene of [27] (dot–dashed line).

R_{JUN} is in the order of 100 $\Omega \cdot \mu$m or less, hence it is much smaller than the measured R_C (symbols). In the worst case ($D_{AC} = 250$ eV), R_{JUN} is about one tenth of R_C. These simulations allow us to estimate the relative error in the experimental R_C due to the impact of the pseudojunction at the edge contact, that is obtained from Eq. 9 as

$$\varepsilon_r = \frac{R_C - R_{M-G}}{R_C} = -\frac{R_{SH}}{R_C W}\Delta L + \frac{R_{JUN}}{R_C}. \quad (10)$$

In the first term of Eq. 10, $\frac{R_{SH}}{R_C W}$ is in the order of 1 μm^{-1} (see Figs. 8 and 9) and $\Delta L < 10$ nm, making impossible to obtain negative R_C values. Furthermore, from Fig. 12 it can be seen that $\frac{R_{JUN}}{R_C} < 0.1$, indicating that the error related to

R_{JUN} is anyway limited, at least in our study. In particular, neglecting R_{JUN}, the error made is less that 10%, a value that is below the average error due to the R_C extraction procedure with TLM, as reported in Fig. 8(b).

V. Conclusions

It has been shown how the use of TLM to extract the M–G contact resistance may lead to artifacts, like negative R_C values. This is due to the small variation of the V_{DP} value among the GFETs in the same TLM array, that hampers to have the same charge density in the channel of the different GFETs used to extract R_C.

It is possible to suppress this effect by shifting the I_{DS}–V_{DS} characteristics, thus compensating the DP position differences. This largely reduces the errors related to the extracted values. It is also possible to exclude the outliers from the linear regression of R_T data; this further improves the dependability of the extracted R_C, but it has been also demonstrated that the largest source of R_C errors is the above mentioned V_{DP} variability. Furthermore, MC simulations have shown that the metal–induced doping and thus the pseudojunction at the contact edge cannot be the main origin of the negative R_C values reported in the literature.

The developed procedure represents a guideline to extract dependable M–G contact resistance values through TLM structures, thus avoiding negative R_C values. This has been verified also by presenting results for different metal contacts. Concluding, this study helps to assess the techniques to characterize the contact resistance of metal–2D materials stacks, also shading new light on the different contributions to the M–G contact resistance and promoting the better understanding of the physics governing the conduction through the M–G stack.

Acknowledgment

The authors would like to thank Prof. Luca Selmi for fruitful discussions.

References

[1] N. Briggs, S. Subramanian, Z. Lin, X. Li, X. Zhang, K. Zhang, K. Xiao, D. Geohegan, R. Wallace, L.-Q. Chen, M. Terrones, A. Ebrahimi, S. Das, J. Redwing, C. Hinkle, K. Momeni, A. van Duin, V. Crespi, S. Kar and J. A. Robinson, "A roadmap for electronic grade 2D materials", vol. 6, p. 022001, Jan. 2019, DOI: 10.1088/2053-1583/aaf836.

[2] Y. Wu, X. Zou, M. Sun, Z. Cao, X. Wang, S. Huo, J. Zhou, Y. Yang, X. Yu, Y. Kong, G. Yu, L. Liao and T. Chen, "200 GHz Maximum Oscillation Frequency in CVD Graphene Radio Frequency Transistors", *ACS Applied Materials & Interfaces*, vol. 8, no. 39, pp. 25645–25649, Sep. 2016, DOI: 10.1021/acsami.6b05791.

[3] F. Schwierz, J. Pezoldt and R. Granzner, "Two–Dimensional Materials and Their Prospects in Transistor Electronics", *Nanoscale*, vol. 7, pp. 8261–8283, Apr. 2015, DOI: 10.1039/C5NR01052G.

[4] S. Riazimehr, A. Bablich, D. Schneider, S. Kataria, V. Passi, C. Yim, G. S. Duesberg, M. C. Lemme, "Spectral sensitivity of graphene/silicon heterojunction photodetectors", *Solid-State Electronics*, vol. 115, pp. 207–212, 2016, DOI: 10.1016/j.sse.2015.08.023

[5] A. D. Smith, F. Niklaus, A. Paussa, S. Vaziri, A. C. Fischer, M. Sterner, F. Forsberg, A. Delin, D. Esseni, P. Palestri, M. Östling, M. C. Lemme, "Electromechanical Piezoresistive Sensing in Suspended Graphene Membranes" Nano Letters vol. 13, n. 7, pp. 3237-3242, 2013, DOI: 10.1021/nl401352k

[6] B. Sensale-Rodriguez, R. Yan, M. M. Kelly, T. Fang, K. Tahy, W. S. Hwang, D. Jena, L. Liu, H. G. Xing, "Broadband graphene terahertz modulators enabled by intraband transitions", *Nature Communications*, vol. 3, 780, 2012, DOI: 10.1038/ncomms1787

[7] C. Liu, Z. Yu, D. Neff, A. Zhamu, B. Z. Jang, "Graphene-Based Supercapacitor with an Ultrahigh Energy Density", *Nano Letters*, vol. 10, n. 12, pp. 4863-4868, 2010, DOI: 10.1021/nl102661q

[8] J. Wassei, R. B. Kaner, "Graphene, a promising transparent conductor", *Materials Today*, vol. 13, n. 3, pp. 52-59, 2010, DOI: 10.1016/S1369-7021(10)70034-1

[9] P. Khakbaz, F. Driussi, A. Gambi, P. Giannozzi, S. Venica, D. Esseni, A. Gahoi, S. Kataria, M.C. Lemme, "DFT study of graphene doping due to metal contacts", *Proceedings of SISPAD*, pp. 279-282, 2019.

[10] F. Giubileo and A. Di Bartolomeo, "The Role of Contact Resistance in Graphene Field–Effect Devices" *Progress in Surface Science*, vol. 92, no. 3, pp. 143–175, Aug. 2017, DOI: 10.1016/j.progsurf.2017.05.002.

[11] S. Venica, F. Driussi, P. Palestri, D. Esseni, S. Vaziri and L. Selmi, "Simulation of DC and RF Performance of the Graphene Base Transistor", *IEEE Transactions on Electron Devices*, vol. 61, no. 7, pp. 2570–2576, Jun. 2014, DOI: 10.1109/TED.2014.2325613.

[12] Y.–W. Lan, C. M. Torres, X. Zhu, H. Qasem, J. R. Adleman, M. B. Lerner, S.–H. Tsai, Y. Shi, L.–J. Li, W.–K. Yeh and K. L. Wang, "Dual–Mode Operation of 2D Material–Base Hot Electron Transistors", Scientific Reports, vol. 6, p. 32503, Sep. 2016, DOI: 10.1038/srep32503.

[13] A. Meersha, H. B. Variar, K. Bhardwaj, A. Mishra, S. Raghavan, N. Bhat and M. Shrivastava, "Record Low Metal – (CVD) Graphene Contact Resistance Using Atomic Orbital Overlap Engineering", *2016 IEEE International Electron Devices Meeting (IEDM)*, pp. 5.3.1–5.3.4, 2016, DOI: 10.1109/IEDM.2016.7838352.

[14] S. Venica, F. Driussi, A. Gahoi, V. Passi, P. Palestri, M. C. Lemme and L. Selmi, "Detailed Characterization and Critical Discussion of Series Resistance in Graphene–Metal Contacts", *Proc. of International Conference of Microelectronic Test Structures (ICMTS)*, pp. 27–31, 2017, DOI: 10.1109/ICMTS.2017.7954259.

[15] F. Xia, V. Perebeinos, Y.–M. Lin, Y. Wu and P. Avouris, "The Origins and Limits of Metal-Graphene Junction Resistance", *Nature Nanotechnology*, vol. 6, pp. 179–184, Feb. 2011, DOI: 10.1038/nnano.2011.6.

[16] P. Blake, R. Yang, S. V. Morozov, F. Schedin, L. A. Ponomarenko, A. A. Zhukov, R. R. Nair, I. V. Grigorieva, K. S. Novoselov and A. K. Geim, "Influence of Metal Contacts and Charge Inhomogeneity on Transport Properties of Graphene Near the Neutrality Point", *Solid State Communications*, vol. 149, no. 27, pp. 1068–1071, Jul. 2009, DOI: 10.1016/j.ssc.2009.02.039.

[17] R. Nouchi, T. Saito and K. Tanigaki, "Observation of Negative Contact Resistances in Graphene Field–Effect Transistors", *Journal of Applied Physics*, vol. 111, no. 8, p. 084314, Apr. 2012, DOI: 10.1063/1.4705367.

[18] T. Chari, R. Ribeiro–Palau, C. R. Dean and K. Shepard, "Resistivity of Rotated GraphiteGraphene Contacts", *Nano Letters*, vol. 16, pp. 4477–4482, Jul. 2016, DOI: 10.1021/acs.nanolett.6b01657.

[19] N. F. W. Thissen, and R. H. J. Vervuurt, A. J. M. Mackus, J. J. L. Mulders, J.–W. Weber, W. M. M. Kessels and A. A Bol, "Graphene Devices with Bottom–Up Contacts by Area–Selective Atomic Layer Deposition", *2D Materials*, vol. 4, no. 2, p. 025046, Feb. 2017, DOI: 10.1088/2053-1583/aa636a.

[20] W. Wang, M. Muruganathan, J. Kulothungan and H. Mizuta, "Study of Dynamic Contacts for Graphene Nano–Electromechanical Switches", *Japanese Journal of Applied Physics*, vol. 56, no. 4S, p. 04CK05, Mar. 2017, DOI: 10.7567/JJAP.56.04CK05.

[21] S. Venica, F. Driussi, G. Amit, P. Palestri, M. C. Lemme and L. Selmi, "On the adequacy of the Transmission Line Model to describe the graphene–metal contact resistance", *IEEE Transaction on Electron Devices*, vol. 65, n. 4, pp. 1589–1596, 2018, DOI: 10.1109/TED.2018.2802946

[22] S. Venica, F. Driussi, G. Amit, S. Kataria, P. Palestri, M. C. Lemme and L. Selmi, "Reliability analysis of the metalgraphene contact resistance extracted by the Transfer Length Method", *Proc. of International Conference of Microelectronic Test Structures (ICMTS)*, pp. 57–62, 2018, DOI: 10.1109/ICMTS.2018.8383765.

[23] A. Gahoi, S. Wagner, A. Bablich, S. Kataria, V. Passi and M. C. Lemme, "Contact Resistance Study of Various Metal Electrodes with CVD Graphene", *Solid–State Electronics*, vol. 125, pp. 234–239, Nov. 2016, DOI: 10.1016/j.sse.2016.07.008.

[24] A. D. Smith, K. Elgammal, F. Niklaus, A. Delin, A. C. Fischer, S. Vaziri, F. Forsberg, M. Rasander, H. Hugosson, L. Bergqvist, S. Schroder, S. Kataria, M. Östling, M. C. Lemme, "Resistive Graphene Humidity Sensors with Rapid and Direct Electrical Readout", *Nanoscale*, vol. 7, pp. 19099–19109, Oct. 2015, DOI: 10.1039/C5NR06038A.

[25] D. C. Montgomery and G. C. Runger, "Applied Statistics and Probability for Engineers", 3rd Edition, *John Wiley & Sons, Inc.*, 2003.

[26] S. Venica, M. Zanato, F. Driussi, P. Palestri and L. Selmi, "Modeling Electrostatic Doping and Series Resistance in Graphene-FETs",

2016 International Conference on Simulation of Semiconductor Processes and Devices (SISPAD), pp. 357–360, 2016, DOI: 10.1109/SISPAD.2016.7605220.

[27] T. Low, S. Hong, J. Appenzeller, S. Datta, M. S. Lundstrom, “Conductance Asymmetry of Graphene p-n Junction”, *IEEE Transaction on Electron Devices*, vol. 56, pp. 1292–1299, June 2009, DOI: 10.1109/TED.2009.2017646.

[28] P. A. Khomyakov, A. A. Starikov, G. Brocks, P. J. Kelly, “Nonlinear screening of charges induced in graphene by metal contacts”, *Physical Review B*, vol. 82, p. 115437, 2010, DOI: 10.1103/PhysRevB.82.115437.

[29] C. Shen, J. Liu, N. Jiao, C. X. Zhang, H. Xiao , R. Z. Wang, L. Z. Sun, “Transport properties of graphene/metal planar junction”, *Physics Letters A*, vol. 378, pp. 1321–1325, 2014, DOI: 10.1016/j.physleta.2014.03.008.

[30] F. Liu, W. T. Navaraj, N. Yogeswaran, D. H. Gregory, R. Dahiya, “van der Waals Contact Engineering of Graphene Field-Effect Transistors for Large–Area Flexible Electronics”, *ACS Nano*, vol. 13, pp. 3257–3268, 2019, DOI: 10.1021/acsnano.8b09019.

[31] F. Driussi, S. Venica, A. Gahoi, A. Gambi, P. Giannozzi, S. Kataria, M.C. Lemme, D. Esseni, “Improved understanding of metalgraphene contacts”, *Microelectronic Engineering*, vol. 216, p. 111035, June 2019, DOI: 10.1016/j.mee.2019.111035.